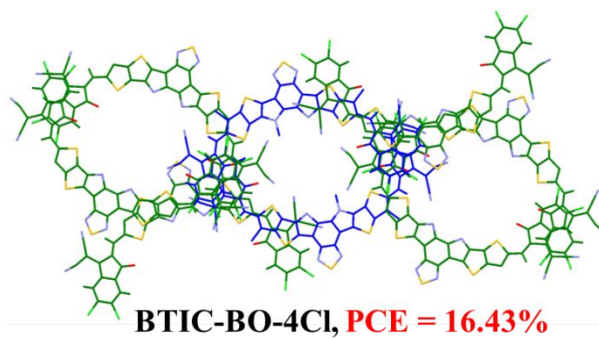


**Alkyl Chain Engineering of Chlorinated Acceptors for
Elevated Solar Conversion**

Journal:	<i>Journal of Materials Chemistry A</i>
Manuscript ID	TA-ART-11-2019-012558.R2
Article Type:	Paper
Date Submitted by the Author:	05-Feb-2020
Complete List of Authors:	Mo, Daize; Southern University of Science and Technology Chen, Hui; Southern University of Science and Technology Zhou, Jiadong; South China University of Technology Tang, Ningning; South China University of Technology Han, Liang; Southern University of Science and Technology Zhu, Yulin; Southern University of Science and Technology Chao, Pengjie; Southern University of Science and Technology Lai, Hanjian; Southern University of Science and Technology Xie, Zengqi; South China University of Technology He, Feng; Southern University of Science and Technology

Table of Contents



A chlorinated acceptor with 2-butyloctyl side chains shows 3D interpenetrated structure in single crystal, and promotes the PCE up to 16.43%.

Alkyl Chain Engineering of Chlorinated Acceptors for Elevated Solar Conversion

Daize Mo,^{‡,a,b} Hui Chen,^{‡,a,c} Jiadong Zhou,^{‡,d} Ningning Tang,^d Liang Han,^a Yulin Zhu,^a

Pengjie Chao,^a Hanjian Lai,^a Zengqi Xie^{*,d} and Feng He^{*,a}

^a Shenzhen Grubbs Institute and Department of Chemistry, Southern University of Science and Technology, Shenzhen 518055, China.

^b Institute of Chinese Medical Sciences, University of Macau, Macao 999078, China.

^c Academy for Advanced Interdisciplinary Studies, Southern University of Science and Technology, Shenzhen 518055, China

^d Institute of Polymer Optoelectronic Materials and Devices, State Key Laboratory of Luminescent Materials and Devices, South China University of Technology, Guangzhou 510640, China.

[‡]These authors contributed equally to this work.

*E-mail: hef@sustech.edu.cn (F.H.); msxiez@scut.edu.cn (Z.X.)

ABSTRACT

Alkyl chain engineering has been widely applied in the preparation of high-performance organic solar conversion materials. In this work, a series of high-performance acceptor-donor-acceptor-donor-acceptor nonfullerene acceptors (NFAs) with different alkyl chain (1-dodecyl, 2-ethylhexyl, 2-butyloctyl, and 2-hexyldecyl) functionalized the core unit and chlorinated end groups are designed and synthesized. All these molecules exhibit strong and broad absorption from 600 to 950 nm, low band gaps (1.34-1.39 eV), and high electron mobility. Furthermore, the single crystal of **BTIC-BO-4Cl** has been successfully grown. From the analysis of its single crystal, this molecule forms a three-dimensional (3D) interpenetrating network due to multiple strong and short S \cdots O, Cl \cdots S, and Cl \cdots π interactions among the adjacent **BTIC-BO-4Cl** molecules. This kind of 3D interpenetrating network should definitely be beneficial for the transport of charge carrier, and thus increase the electron mobility of corresponding acceptor. When blended with donor polymer PBDB-TF, it is found that the chlorinated nonfullerene acceptor with 2-butyloctyl substituted side chains at N positions displays the highest device performance with power conversion efficiency (*PCE*) of 16.43% among those acceptors. Our study demonstrates that the use of branched alkyl chains on the nitrogen atoms is beneficial in this high-efficiency core unit compared to the linear one, and the size of branched alkyl chains also has great effects on the resultant material and corresponding device performances.

INTRODUCTION

Organic solar cells (OSCs) had attracted many attentions from the industry to the academic community, due to its outstanding advantages of low cost, lightweight, large-area and flexibility.¹⁻³ During the long past period, the fullerene and its derivatives were the most widely used acceptors in OSCs.⁴⁻⁸ However, due to its inevitable shortcomings (poor visible absorption, limited energy tune ability, and morphology instability), the power conversion efficiency (PCE) of fullerene-based OSCs was only surpass 11%, much lower than other photovoltaic technologies. In contrast, the nonfullerene acceptors (NFAs) had made great progress since 2015, yielding impressive PCEs over 16% in a single-junction device.⁹⁻¹¹ When compared with the fullerene acceptor, they possessed many significant advantages, such as strong absorption to the near-infrared region, simple synthesis and easily purification, and adjustable energy levels,¹²⁻¹⁶ which also motivated the researchers in the area to put considerable efforts on the NFAs, especially on the fused-ring electron acceptors (FREAs). Basically, the design strategies of FREAs were focused on three aspects: the central fused-ring core, side chain engineering, and the electron-withdrawing end groups,¹⁷⁻²⁰ aiming to tune the absorption wavelength, ionization energy and electron affinity.

As we known, the side chains of NFA molecules were important for their processing capability and device fabrications. It was found that the different alkyl chains showed considerable effect on the photovoltaic properties of NFAs due to their various molecular packing and film morphology. For example, Li group developed a

low band gap acceptor (*m*-ITIC) by the side-chain isomerism engineering on the alkyl-phenyl substituent of ITIC.²¹ Higher film absorption coefficient, larger crystalline coherence, and higher electron mobility was achieved, and consequently boosted fill factor (*FF*) and PCE. Wang and coworkers designed four propeller-shaped TPH-based NFAs with different lengths of branched alkyl side chains at the imide positions.²² The TPH-7 with the longest alkyl chains showed the best photovoltaic property due to its stronger crystallinity and higher charge transport. In addition, the side chains of the terminal groups²³ and the side chains of the π -bridges²⁴ on NFAs performance were also in-depth investigated from the literature. Recently, a high-performance NFA named Y6 was reported and an outstanding PCE of 15.7% was achieved.²⁵ From the molecular structure of Y6, two types of alkyl chains were existence (two branched alkyl chains attached at N atom, and two linear alkyl groups connected at thiophene unit) to provide enough processing capability and good morphology for excellent solar conversion. Lately, the PCE of Y6 family molecule using 3rd-position branched alkyl chains could be further improved to over 16% with ternary device strategy.²⁶ Considering the subtle change of alkyl chains could greatly affect the photovoltaic properties of this high performance NFAs, it should be very important to investigate the effect of different alkyl chains with various types and sizes on the properties of this family molecules, especially understanding their real molecular packing and arrangement.

Therefore, in this work, four NFAs with one longer linear alky chain and three branched alkyl chains, named **BTIC-C12-4Cl**, **BTIC-EH-4Cl**, **BTIC-BO-4Cl**, and

BTIC-HD-4Cl (**Chart 1**), were introduced to study the significance of chlorine-substituted acceptors. In the past three years, our group developed a series of chlorinated polymer donors²⁷⁻²⁹ and acceptors^{30, 31} to explore the role of the chlorination in optimizing the solar conversion. The chlorination in this high performance acceptor-donor-acceptor-donor-acceptor (ADADA) NFAs^{32, 33} would help to reveal the critical issues of such substitution to pump the device performance. The influences of the different alkyl chains on the OSC performance were systematically investigated in parallel in these chlorinated acceptors. It was shown that these four acceptors possessed strong absorption in 600-950 nm, low band gap (1.34-1.39 eV), and high electron mobility. The devices based on the blends of these acceptors and polymer donor PBDB-TF exhibited various PCEs in the range of 9.38% to 16.43%. The optimized PCE was achieved from **BTIC-BO-4Cl** with 2-butyloctyl branched side chains, which showed good solubility and processing capability from chlorobenzene solvent. Based on the dramatic enhancement of PCEs from this system, it could be found out that the alkyl side engineering had a significant influence in tuning the optoelectronic properties and photovoltaic performance of the NFAs. With the proper side chains, eventually we can develop better solar conversion materials with high solar conversion and good processing capability for next real commercial applications.

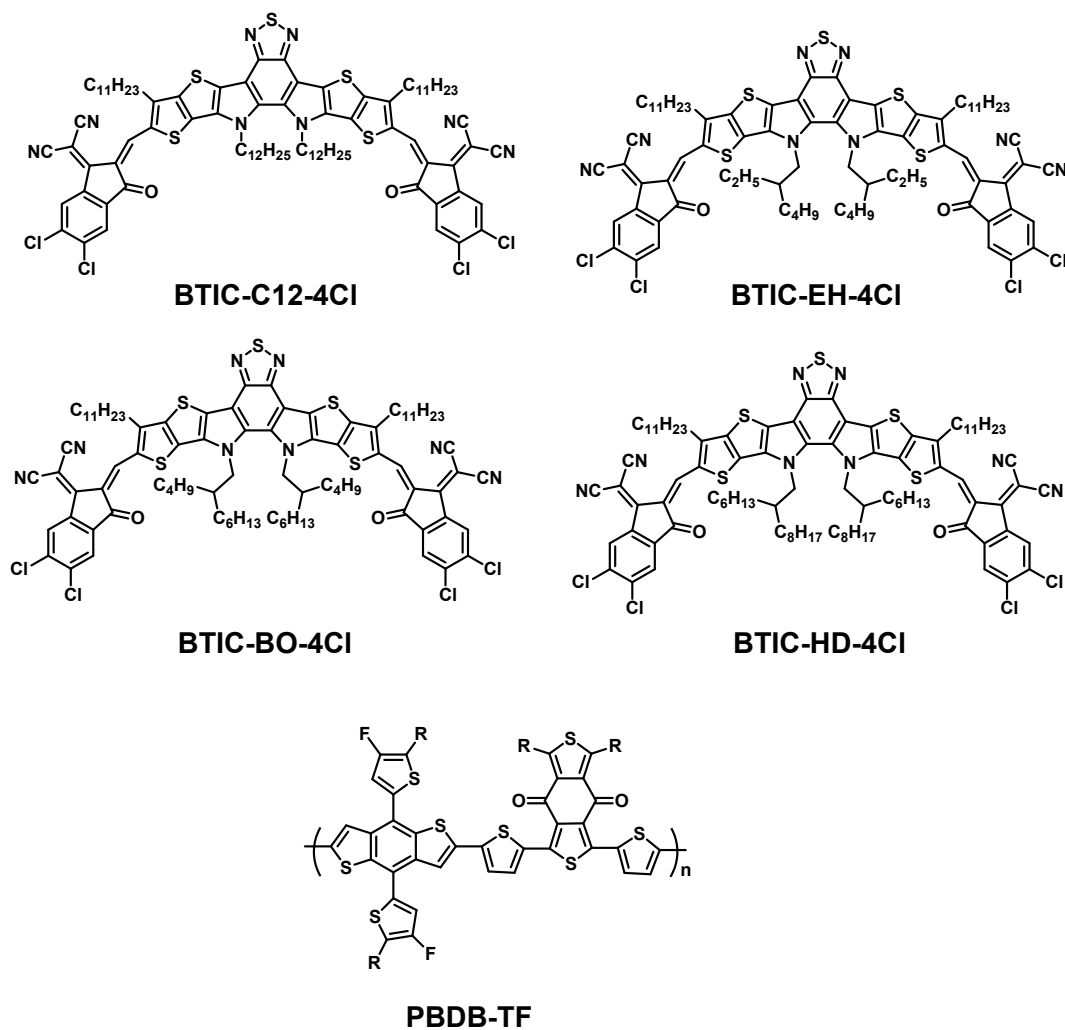


Chart 1. Chemical Structures of **BTIC-C12-4Cl**, **BTIC-EH-4Cl**, **BTIC-BO-4Cl**, **BTIC-HD-4Cl**, and **PBDB-TF**.

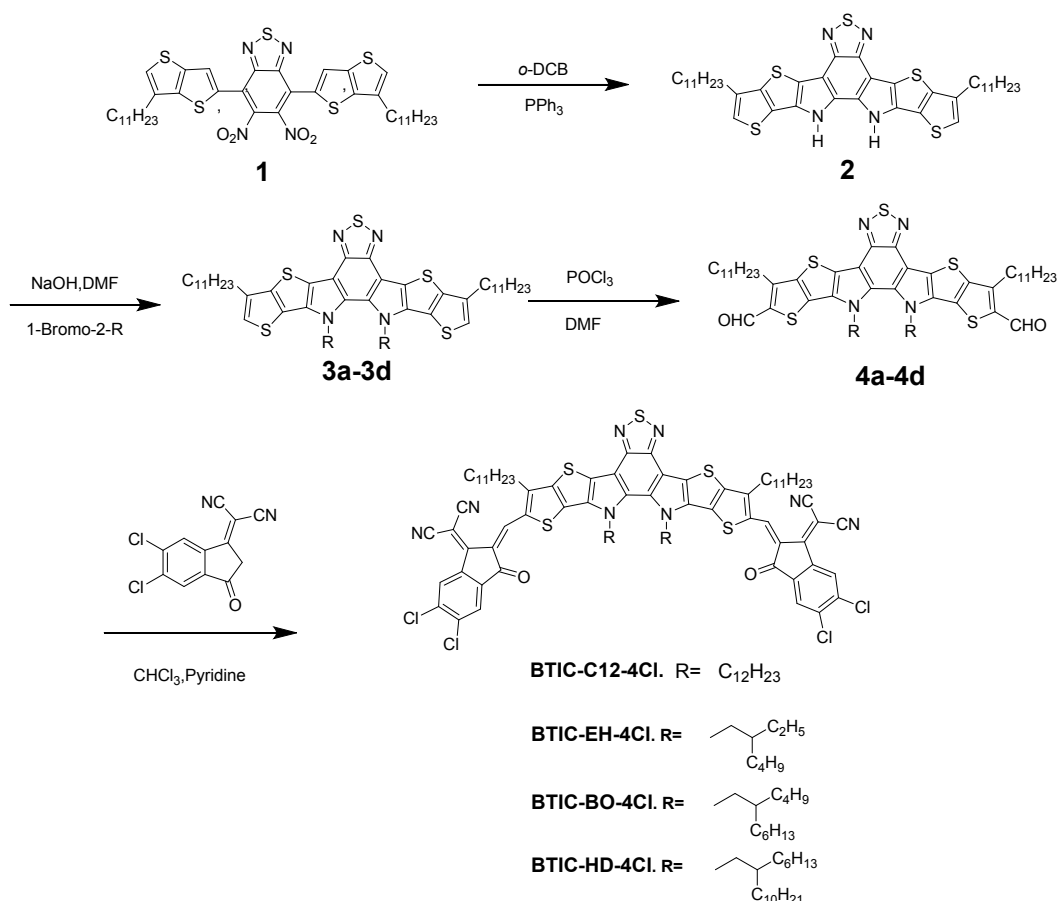
RESULTS

Synthesis and characterization

Chart 1 showed the chemical structures of the four NFAs and polymer donor (PBDB-TF) used in this study. The PBDB-TF:Y6 and PBDB-TF:chlorinated Y6 (named as **BTIC-EH-4Cl**) were easily achieved outstanding PCEs over 15% in the OSCs according to the reported results.^{11,30} However, these two blends especially the **BTIC-EH-4Cl** blend showed limited solubility in some common solvents, such as

chloroform (CF). Herein, three longer alkyl side chains of branched 2-butyloctyl, 2-hexyldecyl, and linear 1-dodecyl were introduced to solve this problem as expected. By this way, we successfully demonstrated that the branched alkyl chain was critical, and the suitable size of branched alkyl chains was of vital importance to their processing capability and photovoltaic performance.

As shown in **Scheme 1**, the Stille coupling of tributyl (6-undecylthieno[3,2-b]thiophene-2-yl)stannane and 4,7-dibromo-5,6-dinitrobenzo[c][1,2,5]-thiadiazole affords compound **1** with high yield (84.8%). Compound **2** was synthesized by the double reductive Cadogan ring closing reaction of compound **1** accompanied with triphenylphosphine (PPh₃) in *o*-dichlorobenzene solvent.³⁴ Compounds **3a-3d** were obtained by alkylation procedure with different brominated alkyl chain using NaOH as base. The dialdehyde compounds **4a-4d** was prepared by the Vilsmeier-Haack reaction by using POCl₃ and DMF with **3a-3d** as orange-red solids. The desired target molecules **BTIC-C12-4Cl**, **BTIC-EH-4Cl**, **BTIC-BO-4Cl**, and **BTIC-HD-4Cl** were finally synthesized with 53-80% yields by Knoevenagel condensation reaction between **4a-4d** with IC-2Cl. It should be noted that here we used another stable and efficient method to synthesize the key intermediate **2** when using PPh₃ as the organophosphorus compound. All intermediates were characterized by ¹H NMR, and the final compounds were further confirmed by high-resolution mass measurements.



Scheme 1. The synthesis of **BTIC-C12-4Cl**, **BTIC-EH-4Cl**, **BTIC-BO-4Cl**, and **BTIC-HD-4Cl**.

The thermal stability of these four acceptors was studied by thermo-gravimetric analysis (TGA) and differential scanning calorimetry (DSC) measurements (**Figure S1**). According to TGA curves, all these four compounds showed good thermal stability with 5% weight loss decomposition temperatures (T_d) varying from 277 to 305.6 °C under nitrogen, which was sufficient to meet the requirement in device fabrication. In the range of 50-250 °C, DSC measurements of them didn't show obvious crystallization and melting peaks, suggesting that the strong intermolecular interactions after the introducing of chlorine atoms. The UV-vis absorption spectra of

the four acceptors were measured in chloroform (CF) solution (10^{-5} mol/L) and in the film state. As shown in **Figure 1a**, these four acceptors had similar strong and broad absorption spectra in the range of 600-850 nm, the absorption peaks of them were all located at 746 nm due to the change of the alkyl chains would not affect the conjugated aromatic backbone. However, various absorption coefficients at maximum absorption peaks for these four molecules were measured (1.55×10^5 L mol $^{-1}$ cm $^{-1}$ for **BTIC-C12-4Cl**, 1.68×10^5 L mol $^{-1}$ cm $^{-1}$ for **BTIC-EH-4Cl**, 2.22×10^5 L mol $^{-1}$ cm $^{-1}$ for **BTIC-BO-4Cl**, and 1.43×10^5 L mol $^{-1}$ cm $^{-1}$ for **BTIC-HD-4Cl**), indicating that the alkyl side chain had a significant influence on the ground state electronic structures.²⁵ The longer branched side chains could lead to larger absorption extinction coefficients which were likely due to their enhanced intermolecular packing properties. In the thin-film state (**Figure 1b**), all the acceptors showed larger red-shifted about 50 nm (**BTIC-C12-4Cl**) and 86 nm (**BTIC-EH-4Cl**, **BTIC-BO-4Cl**, and **BTIC-HD-4Cl**) compared to their absorption peaks in solution. All of the branched alkyl substituted molecules showed nearly the same absorption peaks of 832 nm in thin films, which was much larger than that of the linear alkyl substituted molecule (796 nm). The optical band gaps **BTIC-EH-4Cl**, **BTIC-BO-4Cl**, and **BTIC-HD-4Cl** were measured to be 1.34 eV, while **BTIC-C12-4Cl** was slightly larger at 1.39 eV. The smaller band gap when compared with the linear substituted acceptors implied more ordered aggregations of branched alkyl substituted acceptors. The absorption spectra of the blend films of PBDB-TF:**BTIC-C12-4Cl**, PBDB-TF:**BTIC-EH-4Cl**, PBDB-TF:**BTIC-BO-4Cl**, and PBDB-TF: **BTIC-HD-4Cl** all showed a little blue

shift compared to their pure thin films of these acceptors, as shown in **Figure 1c**. The peak intensity of PBDB-TF:**BTIC-BO-4Cl** (824 nm) in the long-wavelength region is the highest one among the four molecules, indicating the strongest π - π intermolecular interactions in the PBDB-TF:**BTIC-BO-4Cl** blend films. Above all, the broad optical absorption range and high absorption coefficient of **BTIC-BO-4Cl** would be beneficial for its effective utilization of the solar photon.¹¹

The cyclic voltammetry method was conducted to study the electrochemical properties of those four acceptors (**Figure S2**). The onset oxidation potentials (E_{ox})/onset reduction potentials (E_{red}) of **BTIC-C12-4Cl**, **BTIC-EH-4Cl**, **BTIC-BO-4Cl**, and **BTIC-HD-4Cl** were 0.76/-0.64 V, 0.78/-0.61, 0.74/-0.66 V, and 0.78/-0.66 V vs. Ag/Ag⁺, respectively. The corresponding HOMO/LUMO energy levels of them were estimated at -5.56/-4.16 eV, -5.58/-4.19 eV, -5.54/-4.14 eV, and -5.58/-4.14 eV, respectively (**Figure 1d** and **Table 1**). These results implied that the HOMO and LUMO energy levels were mainly determined by the molecular backbone, and the alkyl chain substituted at the N positions had negligible effects on the molecular energy levels of the four molecules. The small ΔE_{HOMO} offset (0.09-0.13 eV) between the four chlorinated acceptors and PBDB-TF donor would provide sufficient driving force for the charge separation and was beneficial in achieving the low energy loss.²⁵ The electrochemical band gaps (E_{g}^{ec}) of **BTIC-C12-4Cl**, **BTIC-EH-4Cl**, **BTIC-BO-4Cl**, and **BTIC-HD-4Cl** were measured to be 1.44, 1.40, 1.40, and 1.40 eV, respectively, very close to their optical band gaps (1.34-1.39 eV).

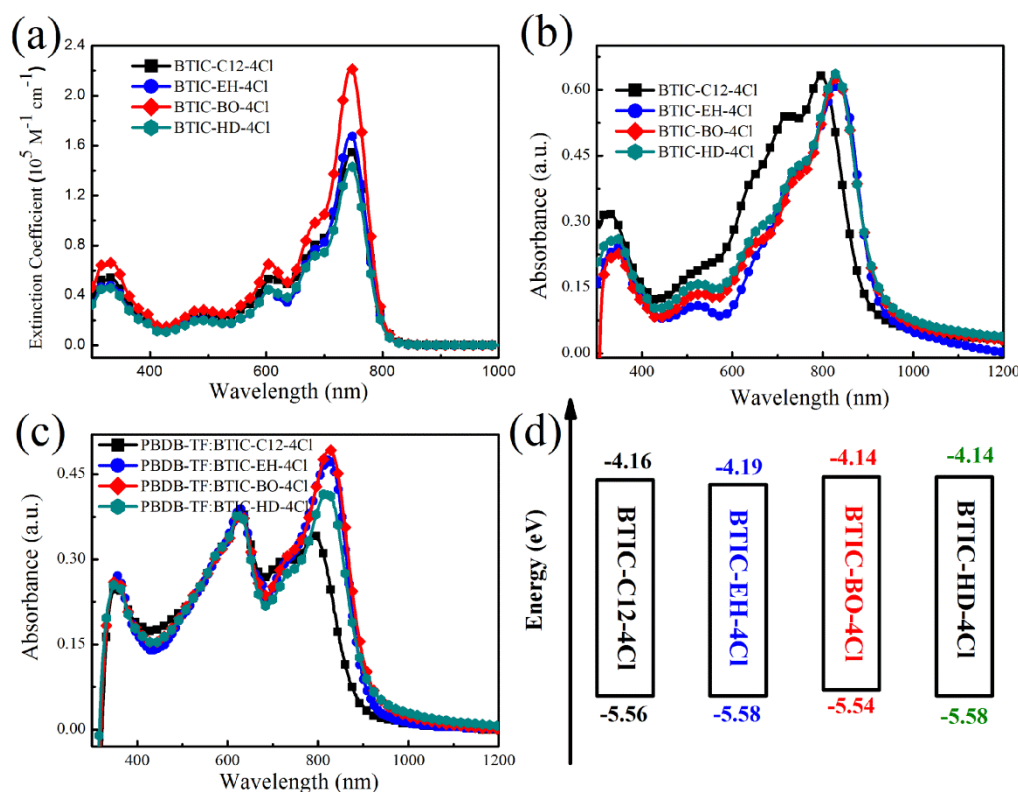


Figure 1. Absorption spectra of **BTIC-C12-4Cl**, **BTIC-EH-4Cl**, **BTIC-BO-4Cl**, and **BTIC-HD-4Cl** in (a) CF solutions and (b) Normalized UV-vis absorption spectra of them in the films; (c) Absorption spectra of the **BTIC-C12-4Cl**: PBDB-TF, **BTIC-EH-4Cl**: PBDB-TF, **BTIC-BO-4Cl**: PBDB-TF, and **BTIC-HD-4Cl**: PBDB-TF films; (d) Energy level diagrams for **BTIC-C12-4Cl**, **BTIC-EH-4Cl**, **BTIC-BO-4Cl**, and **BTIC-HD-4Cl**.

Table 1. Optical and Electrochemical Properties of **BTIC-C12-4Cl**, **BTIC-EH-4Cl**, **BTIC-BO-4Cl**, and **BTIC-HD-4Cl**.

Acceptors	λ_{sol} (nm)	λ_{film} (nm)	λ_{onset} (nm)	ϵ_{max} (L mol ⁻¹ cm ⁻¹)	$E_{\text{g}}^{\text{opt}}$ (eV) ^b	HOMO (eV) ^b	LUMO (eV) ^c	E_{g}^{ec} (eV) ^d
BTIC-C12-4Cl	746	796	890.2	1.55×10^5	1.39	-5.56	-4.16	1.40
BTIC-EH-4Cl	746	832	921.5	1.68×10^5	1.34	-5.54	-4.14	1.40
BTIC-BO-4Cl	746	832	921.5	2.22×10^5	1.34	-5.54	-4.14	1.40
BTIC-HD-4Cl	746	832	921.5	1.43×10^5	1.34	-5.58	-4.14	1.44

^a $E_{\text{g}}^{\text{opt}} = 1240/\lambda_{\text{onset}}$; ^bHOMO = $-(E_{\text{ox}} + 4.74)$; ^cLUMO = $-(E_{\text{red}} + 4.74)$; ^d $E_{\text{g}}^{\text{ec}} = \text{LUMO} - \text{HOMO}$.

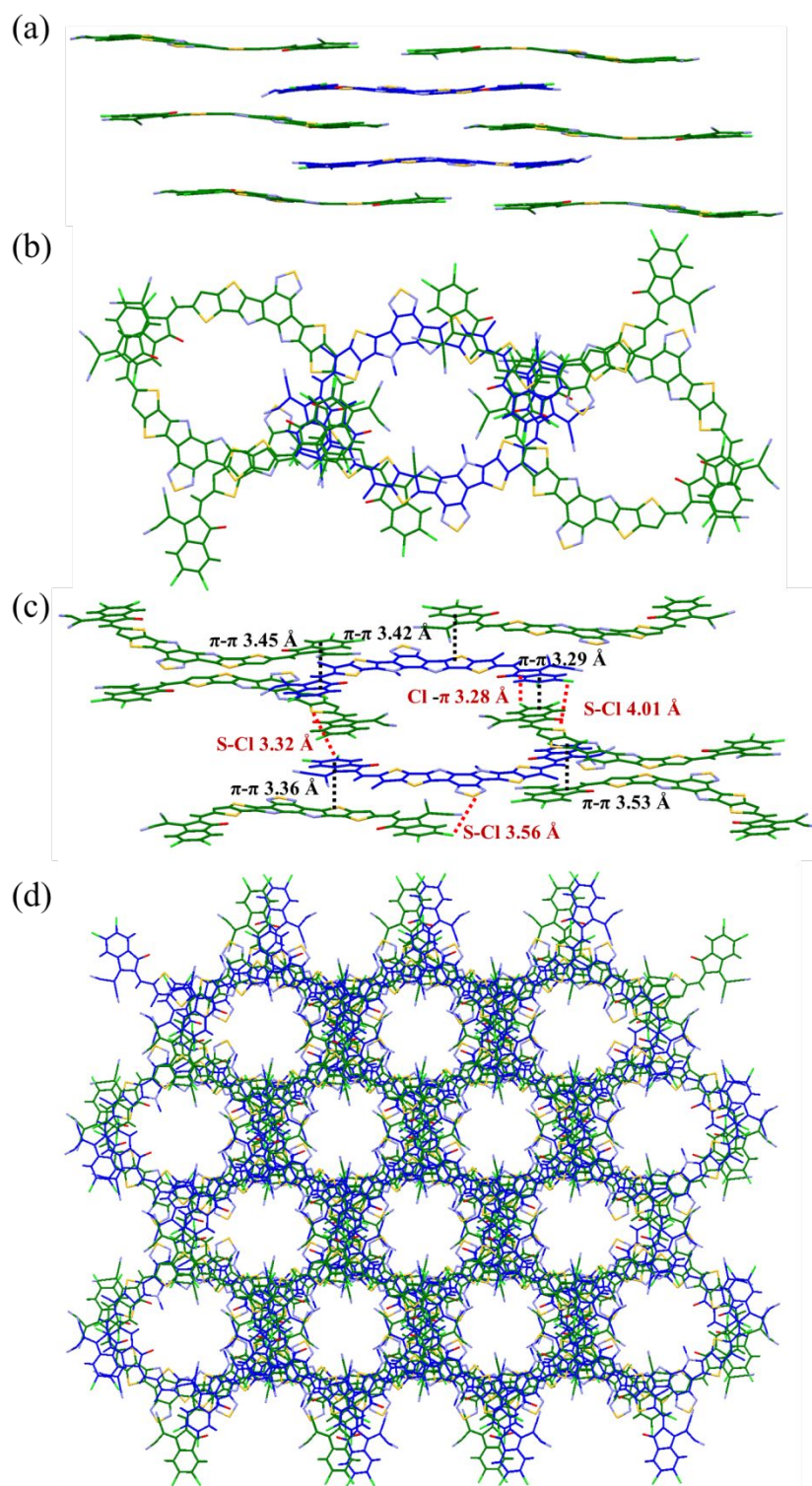


Figure 2. The single crystal structure of **BTIC-BO-4Cl** (2-butyloctyl and n-undecyl side chains were neglected for clarity). (a) Side view of adjacent molecules. (b) Top view of adjacent molecules. (c) The interactions between Cl \cdots S, Cl \cdots π and $\pi \cdots \pi$ of

BTIC-BO-4Cl. (d) Crystal packing diagrams of **BTIC-BO-4Cl** (top view).

In addition, the single crystal of **BTIC-BO-4Cl** was successfully prepared by slow diffusion growth method from the poor solvent ethanol to the good solvent chloroform solution to investigate the molecular configuration and packing behavior (**Figure 2**, and **FigureS4-S6**). As shown in **Figure S4**, the distance of $S \cdots O$ was 2.67 Å in the single **BTIC-BO-4Cl** molecules, which would endow this acceptor good planarity with small dihedral angle of 7.6° between the central core and the dichlorinated end groups. The same two 2-butyloctyl chains on the N atom were situated in completely opposite directions (**FigureS5**), demonstrating that the size of the alkyl chains would greatly influence the packing between the near molecules, especially the length of the side chains. This phenomenon could explain why the choice of different sizes and different types of alkyl chains led to very differently device performance. The 2-butyloctyl chain (**BTIC-BO-4Cl**) and the 1-dodecyl chain (**BTIC-C12-4Cl**) both have the same carbon number, but the π - π distance between the two **BTIC-C12-4Cl** molecules were larger than the **BTIC-BO-4Cl** molecules due to its relatively longer alkyl chain length linear of C12, so its efficiency is much worse than **BTIC-BO-4Cl**. The **BTIC-BO-4Cl** exhibited short π - π distances of 3.29 Å to 3.53 Å between the two adjacent molecules (**Figure 2c**) by the end-group interactions and resulted *J*-aggregation on the whole molecules. Despite two large chlorine atoms at the end groups, the shorter π - π distances of 3.29 and 3.45 Å of the end groups between the two adjacent molecules were still obtained. Especially, the two end groups with π - π distance of 3.29 Å were almost completely overlapped, which was

beneficial to achieve efficient electron hopping between these molecules. Due to the multiple interlocked Cl \cdots S and Cl \cdots π interactions, the π - π distances showed from its single crystal were only about 3.57, 3.56, 4.01, and 3.28 Å, respectively. As shown in **Figure 2d** and **Figure S6**, these interactions allowed **BTIC-BO-4Cl** to present a kind of closed spiral ring microstructures that consists of four molecules in three layers at the vertical direction (**Figure 2a** and **Figure 2b**), each ring was connected with the two adjacent molecules through the strong interactions, so as to eventually form a three-dimensional (3D) interpenetrating network, which could be beneficial for the transport of charge carrier as an acceptor, thus leading to increased electron mobility.

Computational stimulation

To gain deeper insights into the electronic properties and molecular structures of those small molecules, theoretical calculations were carried out using Gaussian 09 at the B3LYP/6-31G(d) level.³⁵ To simplify the calculations, the alkyl groups were replaced by methyl groups. As shown in **Figure S3**, the HOMO energy levels of those acceptors were mainly concentrated on the central cores, and the LUMO levels were widely distributed across the whole molecules and much higher distributed at the dichlorinated end groups. The dihedral angles between the chlorinated end groups and the core were 0.24° in the three molecules, which implied the negligible steric hindrance when the Cl atoms had been designed to the tail end of the NFAs. The LUMO and HOMO energy levels of these acceptors were -3.65 eV and -5.67 eV, respectively. The low HOMO levels indicated that the chlorination strategy on the end groups in the NFAs could efficiently lower the energy levels.

Photovoltaic properties

The effects of the different alkyl chain on the photovoltaic properties of these acceptors were investigated by fabricating BHJ OSCs with a structure of ITO/ZnO/PBDB-TF:acceptor/MoO₃/Ag. Here, PBDB-TF was used as the donor materials due to its strong absorption at 300-750 nm,³⁶ and also matched with the energy levels of these four chlorinated acceptors. **Figure 3a** showed the current density-voltage (*J-V*) curves of OSCs under AM 1.5 G (100 mW cm⁻²) illuminations, and the key device parameters of these four devices were summarized in **Table 2**. The PBDB-TF: **BTIC-C12-4Cl**-based device achieved a PCE of 11.36% with an open circuit voltage (*V*_{oc}) of 0.84 V and a short-circuit current density (*J*_{sc}) of 19.82 mA cm⁻² when CF used as processing solvent. The relatively lower PCE was mainly caused by its low current density. The PBDB-TF: **BTIC-EH-4Cl**-based device showed a PCE of 9.38% due to its limited solubility in CF. In this context, the chlorobenzene (CB) was chosen as the processing solvent, the *V*_{oc} of 0.83 V, both enhanced *J*_{sc} of 25.13 mA cm⁻² and *FF* of 68.64% were achieved, and the PCE was dramatically improved to 14.28% (**Figure S7**). The unsatisfied PCE of this acceptor in CF pushed us to concern that the 2-ethylhexyl substituent was not sufficient to meet the enough solubility of this core structure. Therefore, longer alkyl chains, 2-butyloctyl and 2-hexyldecyl, were introduced to solve this problem. When 2-butyloctyl side chains were introduced, the PBDB-TF: **BTIC-BO-4Cl**-based device showed much higher *J*_{sc} (24.80 mA cm⁻²) and *FF* (72.20 %), and an PCE of 15.13% was obtained from CF. However, when the side chains became a little bit longer in

BTIC-HD-4Cl, a lower PCE of 13.95 % could only be achieved from CF solution. Due to the impressive photovoltaic performance of **BTIC-BO-4Cl**, we also fabricated its devices using CB as processing solvent. It showed further improved *FF* (76.25%) and J_{SC} (25.26 mA cm⁻²), eventually leading to a champion PCE of 16.43% in this system. From these results, we can conclude that the branched alky chains are crucial to get high efficiency in this fused core system, and the device performance will be dramatically improved when the size of the branched side chains are optimized.

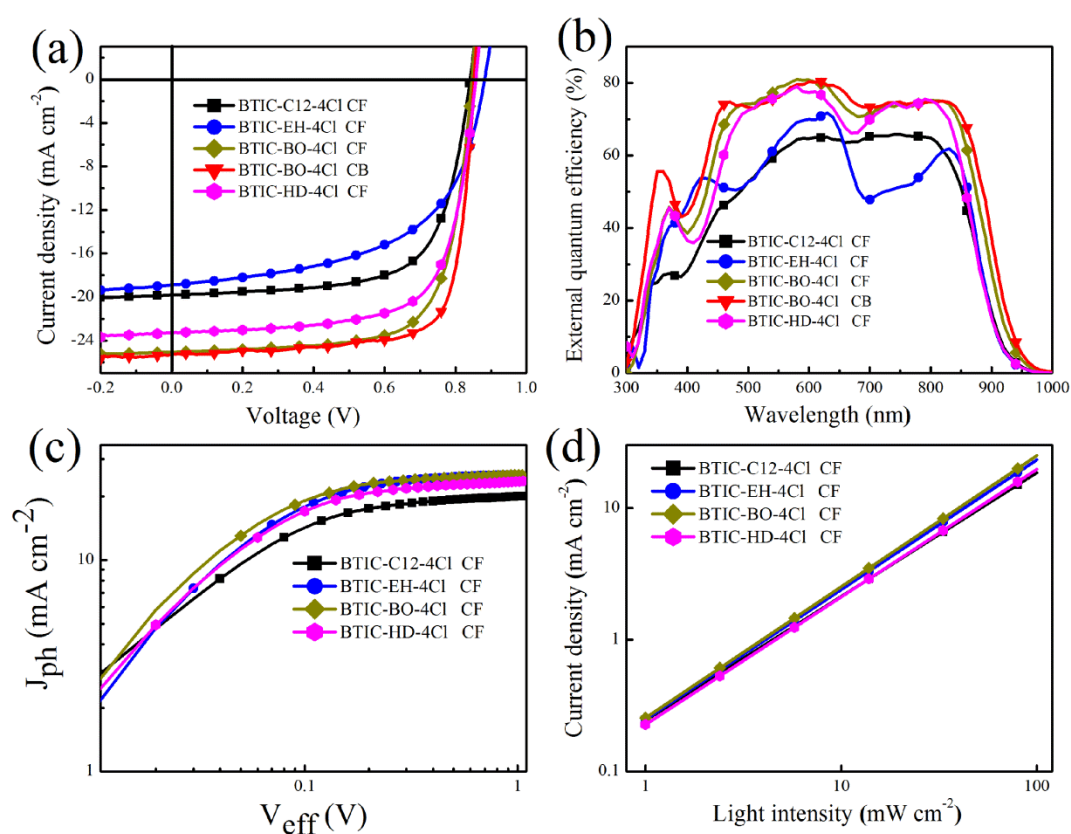


Figure 3. (a) $J-V$ curves of the OSCs based on: **BTIC-C12-4Cl**: PBDB-TF, **BTIC-EH-4Cl**: PBDB-TF, **BTIC-BO-4Cl**: PBDB-TF, and **BTIC-HD-4Cl**: PBDB-TF-based devices; (b) EQE curves of the OSCs based on chlorinated acceptors: PBDB-TF-based devices; (c) The J_{ph} vs V_{eff} and (d) J_{sc} vs light intensity of the chlorinated acceptors-based devices.

Table 2. Detailed photovoltaic parameters of the OSCs.

Acceptors	V_{OC} (V)	J_{SC} (mA cm ⁻²)	FF (%)	PCE (%)
BTIC-C12-4Cl	0.84	19.82	68.27	11.36
(CF)	(0.85±0.002)	(19.76±0.09)	(67.25±0.70)	(11.16±0.12)
BTIC-EH-4Cl	0.88	18.90	56.24	9.38
(CF)	(0.88±0.001)	(18.75±0.12)	(55.74±0.80)	(9.18±0.13)
BTIC-EH-4Cl	0.83	25.13	68.64	14.28
(CB)	(0.83±0.001) ^a	(24.90±0.22)	(69.16±0.92)	(14.04±0.16)
BTIC-BO-4Cl	0.85	24.80	72.20	15.13
(CF)	(0.85±0.001)	(24.64±0.18)	(71.35±0.76)	(14.94±0.11)
BTIC-BO-4Cl	0.85	25.26	76.25	16.43
(CB)	(0.85±0.002) ^a	(25.18±0.36)	(75.61±0.80)	(16.19±0.16)
BTIC-HD-4Cl	0.86	23.24	69.78	13.95
(CF)	(0.85±0.002)	(23.12±0.12)	(69.16±0.89)	(13.75±0.15)

The E_{loss} are calculated to be 0.65, 0.58, 0.61, and 0.63 eV for the devices based on **BTIC-C12-4Cl**, **BTIC-EH-4Cl**, **BTIC-BO-4Cl**, and **BTIC-HD-4Cl**, respectively, where E_{loss} is defined as $E_{loss}=E_g-eV_{OC}$ (E_g of the blend films were determined from the intersection of the extrapolated EQE edge and the local EQE maximum at the edge of the EQE spectrum)^{37, 38}. It can be found that the E_{loss} of the three branched acceptors (0.48-0.63 eV) were all smaller than that of **BTIC-C12-4Cl**-based device (0.65 eV). Due to their lower E_{loss} , the three branched acceptors could still maintain a relatively high V_{OC} in the case of significantly broadening their spectral range. Compared with other three acceptors, **BTIC-BO-4Cl**-based devices show higher J_{SC} , and FF values. Higher J_{SC} is related to the balanced intermolecular interactions of the different alkyl chains, and higher FF was due to the higher mobility and favorable morphology of the blend films. The improved J_{SC} values of PBDB-TF:**BTIC-BO-4Cl**

was also further evidenced by the external quantum efficiency (EQE) curves. As shown in **Figure 3b**, all of these devices shown broad response in the EQE curve range (300-930 nm). The PBDB-TF:**BTIC-BO-4Cl**-based device showed broader photo-response than that of other devices, especially in the long-wavelength region. The maximum EQE value of PBDB-TF: **BTIC-BO-4Cl**-based device is 81%, also higher than that of PBDB-TF: **BTIC-HD-4Cl** (79%), PBDB-TF:**BTIC-C12-4Cl** (66%), and PBDB-TF: **BTIC-EH-4Cl** (71.7%)-based devices, indicating more efficient charge generation and collection in PBDB-TF: **BTIC-BO-4Cl**-based OSCs. The integrated J_{SC} from the EQE spectra of **BTIC-C12-4Cl**(CF), **BTIC-EH-4Cl**(CF), **BTIC-BO-4Cl**(CF), **BTIC-BO-4Cl**(CB), and **BTIC-HD-4Cl**(CF) were calculated to be 18.99, 18.72, 23.73, 24.58, and 22.26 mA cm⁻², respectively, very close to the values obtained from the J - V measurements (< 5% error).

The diagrams of photocurrent (J_{ph}) vs effective voltage (V_{eff}) of those devices were also investigated to study the excitation dissociation and charge collection process of the four devices (**Figure 3c**). J_{ph} was defined as $J_L - J_D$, J_L was the current densities under illumination, and J_D was the current densities under illumination in the dark. V_{eff} was defined as $V_0 - V_a$, V_a was the applied voltage and V_0 was the voltage when the J_{ph} was at zero. All of the four devices reached saturated photocurrent density (J_{sat}) as the V_{eff} arrived at about 1 V, suggested their minimized charge recombination at the higher voltage. In addition, the charge dissociation and charge collection probability $P(E,T)$ values could be calculated via the equation J_{ph}/J_{sat} , which were determined to 90%, 91%, 96%, and 92% for **BTIC-C12-4Cl**, **BTIC-EH-4Cl**,

BTIC-BO-4Cl, and **BTIC-HD-4Cl**-based devices, respectively. The most increased $P(E,T)$ values indicated that **BTIC-BO-4Cl**-based devices exhibit the most efficient charge dissociation and collection processes when compared with those of **BTIC-C12-4Cl**, **BTIC-EH-4Cl**, and **BTIC-HD-4Cl**-based devices.

To further study the charge recombination behavior under the short-circuit condition; the correlations of the J_{SC} versus light density (P) curves were also measured for the four blends (**Figure 3d**), which could be described by the equation $J_{SC} \propto P_{light}^{\alpha}$. The α values of **BTIC-BO-4Cl**-based OSCs were calculated to be 0.99, which is a little higher than that of **BTIC-C12-4Cl** (0.96), **BTIC-EH-4Cl** (0.93), and **BTIC-HD-4Cl** (0.98), demonstrating that bimolecular recombination for **BTIC-BO-4Cl**-based OSCs were weaker than other three devices.

Hole Mobility

The hole and electron mobility of **BTIC-C12-4Cl**, **BTIC-EH-4Cl**, **BTIC-BO-4Cl**, and **BTIC-HD-4Cl** blend films were determined by the space-charge-limited current (SCLC) method with a structure of ITO/PEDOT:PSS/PBDB-TF:acceptor (1.1:1, w/w)/MoO₃/Ag (**Table S1** and **Figure S8**). The hole mobilities of the **BTIC-C12-4Cl**, **BTIC-EH-4Cl**, **BTIC-BO-4Cl**, and **BTIC-HD-4Cl** are 1.9×10^{-4} , 5.7×10^{-5} , 3.6×10^{-4} , and 2.5×10^{-4} cm² V⁻¹ s⁻¹, respectively. The electron mobility was determined to be 8.7×10^{-5} , 7.7×10^{-5} , 2.4×10^{-4} , and 1.1×10^{-4} cm² V⁻¹ s⁻¹, respectively. It was found that **BTIC-BO-4Cl** showed both higher hole and electron mobilities than that of the other three acceptors. At the same time, more balanced hole/electron mobility (μ_h/μ_e) was also obtained from the

PBDB-TF:**BTIC-BO-4Cl** film (1.5), which were about 2.2 for PBDB-TF:**BTIC-C12-4Cl** and 2.3 for PBDB-TF:**BTIC-HD-4Cl**. Higher mobility and charge balance are both favorable for charge transport and efficient carrier collection, which should be beneficial to higher J_{SC} and FF that have showed in the PBDB-TF:**BTIC-BO-4Cl**-based devices.³⁹

Morphological characterization

To further study the morphology of the blend films of these four acceptors, the AFM and TEM measurements were also investigated. As shown in **Figure 4a-4d**, the blended films of PBDB-TF:**BTIC-C12-4Cl**, PBDB-TF:**BTIC-EH-4Cl**, PBDB-TF:**BTIC-BO-4Cl**, and PBDB-TF:**BTIC-HD-4Cl** all exhibit quite smooth and uniform surfaces with similar root-mean-square roughness (RMS) of 0.724, 0.923, 0.773, and 0.773 nm, respectively. The TEM (**Figure 4e-4h**) also shows that all four acceptors exhibit uniform morphology with appropriate domain size. The branched alkyl substituted acceptor blend films showed a little bigger domain size than that of the linear alkyl substituted acceptors. This was likely due to the faster crystallization rate of the **BTIC-EH-4Cl**, **BTIC-BO-4Cl**, and **BTIC-HD-4Cl**, and resulted in a more ordered condensed state and larger phase domain size in the blend films. It could help them to obtain higher phase purities in the branched side chain substituted acceptors, and eventually to elevate J_{sc} and FF in photovoltaic devices.⁴⁰

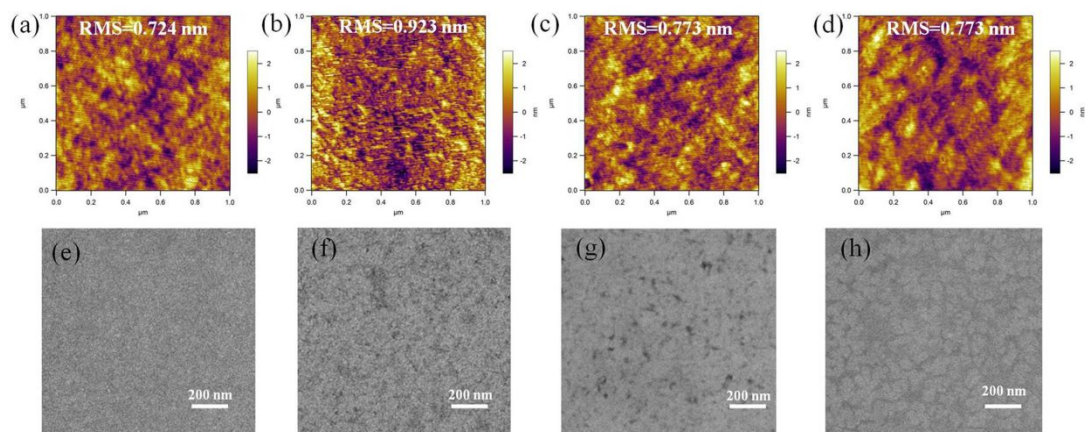


Figure 4. AFM topography images of **BTIC-C12-4Cl: PBDB-TF** (a), **BTIC-EH-4Cl: PBDB-TF** (b), **BTIC-BO-4Cl: PBDB-TF** (c), and **BTIC-HD-4Cl: PBDB-TF** (d) blend films; TEM images of **BTIC-C12-4Cl: PBDB-TF** (e), **BTIC-EH-4Cl: PBDB-TF** (f), **BTIC-BO-4Cl: PBDB-TF** (g), and **BTIC-HD-4Cl: PBDB-TF** (h) blend films.

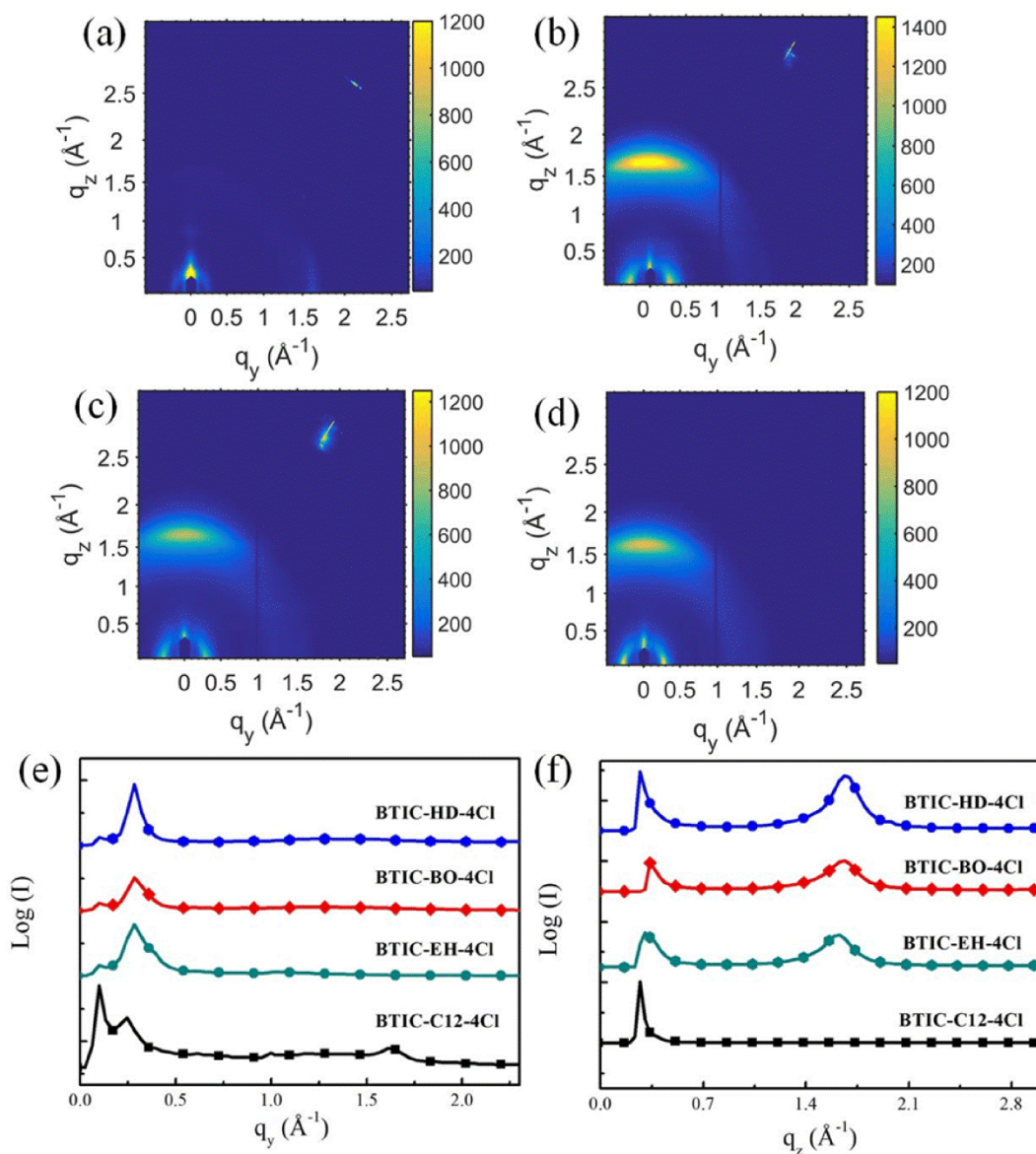


Figure 5. Two-dimensional GIWAXS patterns of PBDB-TF: **BTIC-C12-4Cl** (a), PBDBTF: **BTIC-EH-4Cl** (b), PBDB-TF: **BTIC-BO-4Cl** (c), and PBDB-TF: **BTIC-HD-4Cl** (d) blend films. (e) In-plane line and (f) out-of-plane-cut profiles of GIWAX patterns.

Grazing incidence wide-angle X-ray scattering (GIWAXS) method was used to determine the correlation between the microstructure of the blend films and the photovoltaic performance of the devices. All of the three branched acceptors (**Figure**

5a-5c) show clear (010) diffraction peaks in the out-of-plane direction, suggested the dominant existence of the face-on orientation. While PBDB-TF: **BTIC-C12-4Cl** blend show a predominantly edge-on preferred orientation (π - π distances: 3.9 Å), as shown in **Figure 5d**. In details, the (010) diffraction peaks of PBDB-TF:**BTIC-EH-4Cl**, PBDB-TF:**BTIC-BO-4Cl**, and PBDB-TF:**BTIC-HD-4Cl** showed the π - π distances of 3.9, 3.8 and 3.8 Å in those three blend films (**Figure 5f**), but almost no diffraction peak can be observed in this region of PBDB-TF: **BTIC-C12-4Cl** blend film. In the in plane direction, the lamellar packing distance of PBDB-TF:**BTIC-C12-4Cl**, PBDB-TF:**BTIC-EH-4Cl**, PBDB-TF:**BTIC-BO-4Cl**, and PBDB-TF:**BTIC-HD-4Cl** was determined to be 25.6, 22.2, 22.2, and 22.2 Å, respectively. It implies that PBDB-TF:**BTIC-C12-4Cl** blend film has the largest lamellar packing distance in these four blends due to its longest linear alkyl chain. Therefore, it looks that the incorporation of different length of branched alkyl chains into these acceptors will not obviously affect the intermolecular interactions in the blend films, but the introducing of the linear C12 chain will turn the molecular orientation to edge-on dominated, and thus hinder its performance as the active material in OSCs.

CONCLUSIONS

In conclusion, four chlorinated nonfullerene acceptors with different alkyl chains substituted at the N position, named **BTIC-C12-4Cl**, **BTIC-EH-4Cl**, **BTIC-BO-4Cl**, and **BTIC-HD-4Cl** were synthesized and characterized. The proper branched alkyl substituted molecule could cause larger red-shifted absorption in the films and better

phase separation when compared with the linear alkyl substituted molecule. Based on the single crystal analysis, **BTIC-BO-4Cl** exhibited short π - π distances (3.29 Å-3.53 Å) between the adjacent molecules due to the multiple interlocked Cl \cdots S and Cl \cdots π interactions. Because of the S \cdots O, Cl \cdots S, and Cl \cdots π interactions, this nonfullerene acceptor formed a 3D interpenetrating network, and leading to high electron mobility. As a result, the acceptor with 2-butyloctyl side chains (**BTIC-BO-4Cl**) delivered a champion PCE of 16.43% by combining with PBDB-TF due to its short π - π stacking distance, good morphology formation, and better charge transport property. The linear alkyl substituted molecule (**BTIC-C12-4Cl**) only showed a much lower PCE of 11.36% in the parallel device tests. All these results indicate that the great potential of chlorinated end-capping nonfullerene acceptor for high efficient polymer solar cells, and the alkyl chain engineering plays very important role in those systems with strong non-covalent intermolecular interactions to optimize the final device performance.

Conflicts of interest

There are no conflicts to declare.

Acknowledgements

This work was financially supported by the National Natural Science Foundation of China (51773087, 21733005, 21975115), Shenzhen Fundamental Research Program (KQJSCX20180319114442157, JCYJ20170817111214740, JCYJ20180302180238419) and Shenzhen Nobel Prize Scientists Laboratory Project (C17213101), and the Guangdong Innovative and Entrepreneurial Research

Team Program under contract no. 2016ZT06G587. We thank Dr. Joseph Strzalka and Dr. Zhang Jiang for the assistance with GIWAXS measurements. Use of the Advanced Photon Source (APS) at the Argonne National Laboratory was supported by the U.S. Department of Energy, Office of Science, Office of Basic Energy Sciences, under contract No. DE-AC02-06CH11357. We also thank the SUSTech Core Research Facilities for the AFM and TEM measurements.

Notes and references

1. G. Li, R. Zhu and Y. Yang, *Nat. Photonics.*, 2012, **6**, 153-161.
2. O. Inganäs, *Adv. Mater.*, 2018, **30**, 1800388.
3. A. Wadsworth, M. Moser, A. Marks, M. S. Little, N. Gasparini, C. Brabec, D. Baran and I. McCulloch, *Chem. Soc. Rev.*, 2019, **48**, 1596-1625
4. Y. H. Liu, J. B. Zhao, Z.K. Li, C. Mu, W. Ma, H.W. Hu, K.Jiang, H.R.Lin, H.Ade and H.Yan, *Nat. Commun.*, 2014,**5**, 5293-5210.
5. J.B. Zhao, Y.K. Li, G.F. Yang, K. Jiang, H.R Lin, H.Ade, W. Ma and H.Yan. *Nat. Energy* 2016, **1**, 15027-15033.
6. C.C. Chen, W.H.Chang, K.Yoshimura, K. Ohya, J.B.You, J. Gao, Z.R. Hong and Y. Yang, *Adv. Mater.*, 2014, **26**, 5670-5677.
7. Z.C. He, B. Xiao, F. Liu, H.B. Wu, Y.L.Yang, S. Xiao, C.Wang, T. P. Russell and Y. Cao, *Nat. Photonics*, 2012, **6**, 593-597.
8. H.Q. Zhou, Y. Zhang, C.K. Mai, S. D. Collins, G. C. Bazan , T. Q. Nguyen and A. J. Heeger, *Adv. Mater.*, 2015, **27**, 1767-1773.

9. Q.S. An, X.L. Ma, J.H. Gao, F.J. Zhang, *Sci. Bull.*, 2019, **64**, 64504-506.
10. R.N. Yu, H.F. Yao, Y. Cui, L. Hong, C. He and J.H. Hou, *Adv. Mater.*, 2019, **36**, 1902302.
11. Y. Cui, H.F. Yao, J.Q. Zhang, T. Zhang, Y.M. Wang, L. Hong, K.H. Xian, B.W. Xu, S.Q. Zhang, J. Peng, Z.X. Wei, F. Gao and J.H. Hou, *Nat. Commun.*, 2019, **10**, 2515
12. S.M. McAfee, J.M. Topple, I.G. Hill and G.C. Welch, *J. Mater. Chem. A.*, 2015, **3**, 16393-16408.
13. C.B. Nielsen, S. Holliday, H.Y. Chen, S.J. Cryer and I. McCulloch, *Acc. Chem. Res.*, 2015, **48**, 2803-2812.
14. S.X. Li, W. Liu, C.Z. Li, M.M. Shi and H.Z. Chen, *Small*, 2017, **13**, 1701120.
15. J.H. Hou, O. Inganäs, R. H. Friend and F. Gao, *Nat. Mater.*, 2018, **17**, 119-128.
16. Y.K. Yang, Z.G. Zhang, H.J. Bin, S.S. Chen, L. Gao, L.W. Xue, C.D. Yang and Y. F. Li, *J. Am. Chem. Soc.*, 2016, **138**, 15011-15018.
17. T.F. Li, S.X. Dai, Z.F. Ke, L.X. Yang, J.Y. Wang, C.Q. Yan, W. Ma and X.W. Zhan, *Adv. Mater.*, 2018, **30**, 1705969.
18. B. Kan, H.R. Feng, X.J. Wan, F. Liu, X. Ke, Y.B. Wang, Y.C. Wang, H.T. Zhang, C.X. Li, J.H. Hou and Y.S. Chen, *J. Am. Chem. Soc.*, 2017, **139**, 4929-4934.
19. J.Y. Wang, W. Wang, X.H. Wang, Y. Wu, Q.Q. Zhang, C.Q. Yan, W. Ma, W. You and X.W. Zhan, *Adv. Mater.*, 2017, **29**, 1702125.
20. J.Y. Wang, J.X. Zhang, Y.Q. Xiao, T. Xiao, R.Y. Zhu, C.Q. Yan, Y.Q. Fu, G.H. Lu, X.H. Lu, S. R. Marder and X.W. Zhan, *J. Am. Chem. Soc.*, 2018, **140**, 9140-9147.

21. Y.K. Yang, Z.G. Zhang, H.J. Bin, S.S. Chen, L. Gao, L.W. Xue, C.D. Yang, and Y.F. Li, *J. Am. Chem. Soc.*, 2016, **138**, 15011-15018.
22. H.T. Fu, D. Meng, X.Y. Meng, X.B. Sun, L.J. Huo, Y.Z. Fan, Y. Li, W. Ma, Y.M. Sun, and Z.H. Wang, *J. Mater. Chem. A.*, 2017, **5**, 3475-3482.
23. J. Zhu, S.S. Li, X.Y. Liu, H.F. Yao, F.H. Wang, S.Q. Zhang, M.L. Sun, and J.H. Hou, *J. Mater. Chem. A.*, 2017, **5**, 15175-15182.
24. S.L. Ming, C.E. Zhang, P.C. Jiang, Q.L. Jiang, Z.F. Ma, J.S. Song, and Z.S. Bo, *ACS Appl. Mater. Interfaces*, 2019, **11**, 19444-19451.
25. J. Yuan, Y.Q. Zhang, L.Y. Zhou, G.C. Zhang, H.H. Yip, T.K. Lau, X.H. Lu, C.Zhu, H.J. Peng, P.A. Johnson, M. Leclerc, Y. Cao, J. Ulanski, Y.F. Li and Y.P. Zou, *Joule*, 2019, **3**, 1140-1151.
26. K. Jiang, Q.Y. Wei, J.Y. Lin Lai, Z.X. Peng, H.K. Kim, J. Yuan, L. Ye, H. Ade, Y.P. Zou, and H. Yan. *Joule*, 2019, **3**, 3020-3033.
27. D.Z. Mo, H. Wang, H. Chen, S.W. Qu, P.J. Chao, Z. Yang, L.L. Tian, Y.A. Su, Y. Gao, B. Yang, W. Chen and F. He. *Chem. Mater.*, 2017, **29**, 2819-2830.
28. Z.M. Hu, H. Chen, J.F. Qu, X.W. Zhong, P.J. Chao, M. Xie, W. Lu, A.H. Liu, L.L. Tian, Y.A. Su, W. Chen and F. He, *ACS Energy Lett.*, 2017, **2**, 753-758.
29. H. Wang, P.J. Chao, H. Chen, Z. Mu, W. Chen and F. He, *ACS Energy Lett.*, 2017, **2**, 1971-1977.
30. J.F. Qu, Q.Q. Zhao, J.D. Zhou, H.J. Lai, T. Liu, D.N. Li, W. Chen, Z.Q. Xie and F. He, *Chem. Mater.*, 2019, **31**, 1664-1671.
31. J.F. Qu, H. Chen, J.D. Zhou, H.J. Lai, T. Liu, P.J. Chao, D.N. Li, Z.Q. Xie, F. He

- and Y.G. Ma, *ACS Appl. Mater. Interfaces*, 2018, 10, 39992-40000.
32. J.H. Miao, J.X. Wang, B. Meng, J. Liu, and L.X. Wang. *Mater. Chem. Front.*, 2018, **2**, 2333-2339.
33. J.H. Miao, B. Meng, J. Liu, and L.X. Wang. *Chem. Commun.*, 2018, **54**, 303-306.
34. S. Ghosh, S. Das, N.R. Kumar, A. R. Agrawal and S. S. Zade, *New J. Chem.*, 2017, **41**, 11568-11575.
35. T. Körzdörfer and J. L. Brédas, *Acc. Chem. Res.*, 2014, **47**, 3284-3291.
36. M.J. Zhang, X. Guo, W. Ma, H. Ade and J.H. Hou, *Adv. Mater.*, 2015, **27**, 4655-4660.
37. V.C. Nikolis, J. Benduhn, F. Holzmueller, F. Piersimoni, M. Lau, O. Zeika, D. Neher, C. Koerner, D. Spoltore, and K. Vandewal, *Adv. Energy Mater.*, 2017, **7**, 1700855.
38. B.B. Fan, X.Y. Du, F. Liu, W.K. Zhong, L. Ying, R.H. Xie, X.F. Tang, K. An, J.M. Xin, N. Li, W. Ma, C.J. Brabec, F. Huang, Y. Cao, *Nat. Energy.*, 2018, **3**, 1051-1058.
39. H. Chen, Z.M. Hu, H. Wang, L.Z. Liu, P.J. Chao, J.F. Qu, W. Chen, A.H. Liu and F. He, *Joule*, 2018, **2**, 1623-1634.
40. W. Gao, Q.S. An, C. Zhong, Z.H. Luo, R.J. Ming, M.Zhang, Y. Zou, F. Liu, F.J Zhang and C.L. Yang, *Chem. Sci.*, 2018, **9**, 8142-8149.